Observations of glories above arctic boundary layer clouds to identify cloud phase

F. Kanngießer[1,2], A. Ehrlich[1] and M. Wendisch[1]

[1] Institute for Meteorology, Stephanstr. 3, 04103 Leipzig
[2] now at: Chalmers University of Technology, Department for Space, Earth and Environment, SE-412 96 Gothenburg, Sweden, E-Mail: franz.kanngiesser@chalmers.se

Abstract

The glory is an optical phenomenon observed above liquid water clouds and consists of coloured rings around the anti-solar point. Since the glory is caused by scattering on spherical particles it can be used as a proxy to identify liquid water at the cloud top. Images taken with a CANON digital camera equipped with a fish-eye lens on board the research aircraft Polar 5 during the measurement campaign Radiation-Aerosol-Cloud Experiment in the Arctic Circle (RACEPAC) were analysed for glories. To identify glories an algorithm consisting of five criteria was developed by using simulations of the scattering angle dependent radiance and a test data set of measurements. The algorithm was tested and proved to be able to distinguish between images showing a glory and images not showing any glory.

Zusammenfassung

Die Glorie ist eine optische Erscheinung, die über Flüssigwasserwolken beobachtet werden kann und aus farbigen Ringen um den Gegensonnenpunkt besteht. Da die Glorie durch Streuung an sphärischen Partikeln entsteht, kann sie zur Identifikation von Flüssigwasser am Wolkenoberrand genutzt werden. Bilder, die mit einer CANON Digitalkamera, die mit einem Fischaugenobjektiv ausgestattet war, von Bord des Forschungsflugzeugs Polar 5 während der Messkampagne RACEPAC aufgenommen worden, wurden auf das Auftreten von Glorien untersucht. Zur Identifikation wurde ein Algorithmus mit fünf Kriterien entwickelt, die mit Hilfe von Simulationen der streuwinkelabhängigen Radianz und einem Testdatensatz der Messungen erstellt wurden. Der Algorithmus wurde getestet und ist in der Lage zwischen Bildern mit und ohne Glorie zu unterscheiden.

1. Introduction

The radiative energy budget is strongly influenced by clouds. While low altitude clouds in low and mid-latitudes have a cooling effect, low clouds in high latitudes may act both cooling and warming e.g. due to the lower altitude of the sun (Wendisch et al., 2013). Previous research has shown that a relatively large proportion of clouds in the Arctic boundary layer are mixed-phase especially in the boundary layer (Mioche et al., 2015). A typical Arctic mixed-phase cloud has an inhomogeneous horizontal distribution of areas consisting of either pure liquid water or pure ice and areas consisting of both liquid water and ice in between the areas of pure phase cloud particles. The patches of pure phase cloud particles have a size range of 100 to 1000 m (Korolev et al., 2003, Korolev and Isaac, 2008). Unlike the horizontal phase distribution the vertical phase distribution is much more structured. The top of Arctic mixed-phase clouds is typically dominated by liquid water

droplets (Ehrlich et al., 2009).
The thermodynamic phase of a cloud can be distinguished by different types of remote sensing, like active remote sensing using lidar or radar or passive remote sensing using microwave radiometers. The approach used here applies passive remote sensing of solar radiation using the directional information. Directional information relies on optical phenomena hence single scattering gives only information concerning the cloud top. This method was previously used by Ehrlich et al. (2012) and by Bréon and Goloub (1998), who used satellite data. Ehrlich et al. (2012) used a digital camera by Canon to retrieve both optical thickness and effective radius of an arctic boundary layer cloud using the cloud bow.
In this study the optical phenomenon of the glory is used as a proxy for the dominating phase at the cloud top. The glory is a backscattering phenomenon which only occurs on spherical particles (Laven, 2005). Since only liquid water droplets are spherical the detection of the glory does allow determining the dominating cloud phase. Basis for the identification was the measured reflected radiance.

2. Instrumentation

With a digital camera (Canon EOS 1D Mark III) with a 180° fish-eye lens (SIGMA 8mm F3.5 EX DG FISHEYE) which was mounted on the Polar 5 research aircraft images displaying the entire half space beneath the aircraft were taken. With the help of a radiometric calibration and an attitude correction each image was converted to scattering angle dependent radiance in different zenith and azimuth direction. In combination with the solar position (θ_0, φ_0) each viewing direction $(\theta_\mathrm{r}, \varphi_\mathrm{r})$ can be converted into a scattering angle using the methods and algorithms described by Ehrlich et al. (2012). Assuming both rotation symmetry and single scattering a scattering angle ϑ was assigned to each pixel by:

$$\vartheta = 180° - \arccos(-\sin\theta_0 \cdot \cos\varphi_0 \cdot \sin\theta_\mathrm{r} \cos\varphi_\mathrm{r} - \sin\theta_0 \cdot \sin\varphi_0 \cdot \sin\theta_\mathrm{r} \cdot \sin\varphi_\mathrm{r} + \cos\theta_0 \cdot \cos\theta_\mathrm{r}) \quad (1)$$

3. Simulation of scattering angle dependent radiance

To analyse the sensitivity of the scattering angle dependent radiance of clouds and to detect glories simulations of radiances of liquid water and ice clouds were produced using the library for radiative transfer libRadtran 2.0.1 (Emde et al., 2016). The radiative transfer calculations were performed with the help of the intensity corrected radiative transfer solver DISORT by Buras et al. (2011). For the ice clouds the ice crystal parametrization for solid columns by Key et al. (2002) was used. The results of the calculations of the radiance $I(\theta, \varphi)$ were then interpolated on a grid representing the whole observed hemisphere. Therefore, the simulated radiances could be converted to scattering angle dependent radiance I(ϑ) like the images of the digital camera.
Fig. 1 shows the simulated scattering angle dependent radiances of liquid water clouds and an ice cloud. To simulate the radiances of liquid water clouds a monodisperse droplet distribution with an effective radius of 10 µm and 4 µm respectively was used. Additionally the cloud optical thickness was varied. The radiances of the ice cloud were simulated by assuming an effective radius of 50 µm and using said ice crystal parametrization. The differences between the ice cloud's radiances after varying optical thickness and/or effective radius were too small to be distinguished in the plot. The scattering angle dependent

radiances of both liquid water and ice clouds differ from the respective phase functions. Despite this fact a glory is detectable at a scattering angle of 180° within the measurements of the scattering angle dependent radiance. In case of ice clouds no glory is observable. With increasing cloud optical thickness the values of the radiance increase as well. From the results shown in Fig. 1 can be concluded additionally that an increase in the effective radius yields an increase in the local maximum near backscattering direction.

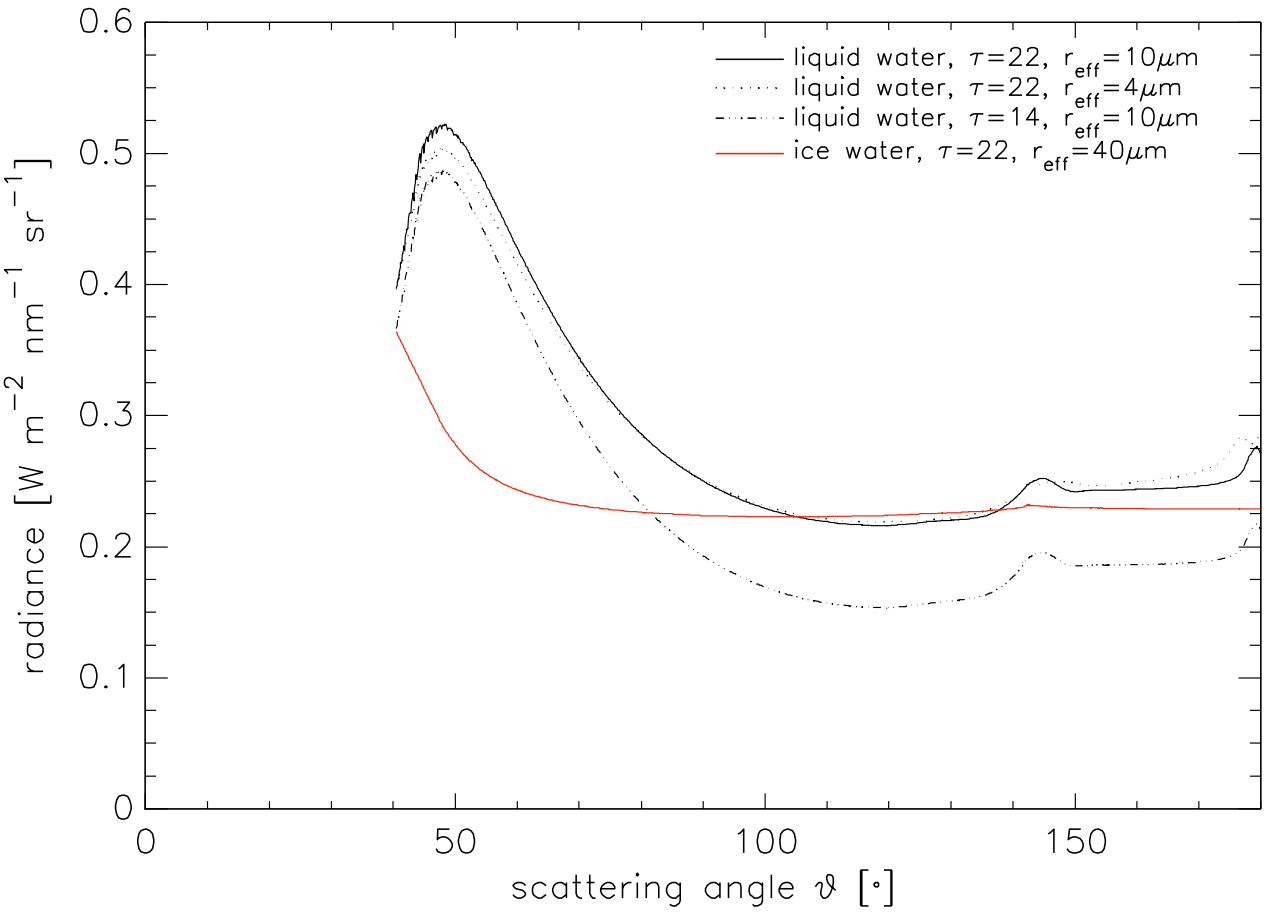

Fig. 1: Simulation results of reflected scattering dependent radiances for liquid water clouds (black) and ice water clouds (red)

4. Definition of Algorithm

As simulations of the scattering angle dependent radiance show the differences between ice and liquid water clouds are especially pronounced in the backscattering direction near 180°. To reduce the potential influence of horizontal inhomogeneities in the phase distribution the range of scattering angles in the development of an identification algorithm was limited to 170°-180°. Focusing only on the maximum in backscattering direction does not allow identifying the glory. Further tests have shown that a single parameter is not sufficient to identify the glory and correspondingly the cloud phase. Therefore, several criteria were defined. The local maximum of the scattering angle dependent radiance between 173° and 180° has to be within the range of 176° and 180°. During the next step it was checked, if the mean of the radiance values ± 0.3° around the maximum minus one per cent of its value ($I_{\max} - 0.01 \cdot I_{\max}$) is larger than the mean of the scattering angle dependent radiance between 173° and 180°. The mean of the maximum $\pm 0.3°$ was chosen to smooth possible irregularities in the measured radiance. This criterion serves as a measure of the maximums

and the glories strength. The two discussed criteria can be expressed as:

$$176° \leq \theta_{\max} \leq 180° \quad (2)$$

$$I_{\max} - 0,01 \cdot I_{\max} > \bar{I}_{173°-180°} \quad (3)$$

Fig. 1 shows a comparison of liquid water clouds and ice clouds. The values for the criteria of the liquid water and ice clouds used in the simulations are listed in the following table. Additionally to the radiances depicted in Fig. 1 the values of simulation results for two more ice clouds are shown in Tab 1. Since the radiances of the ice clouds appeared to be indistinguishable by eye those two additional radiances were not shown in Fig. 1.

Tab. 1 Identification criteria from simulation

		$\theta_{\max}$	$I_{\max} - 0.01 I_{\max}$ [$\mathrm{Wm^{-2}\,nm^{-1}\,sr^{-1}}$]	$\bar{I}_{173°-180°}$ [$\mathrm{Wm^{-2}\,nm^{-1}\,sr^{-1}}$]
liquid water cloud	$\tau = 22, r_{\mathrm{eff}} = 4\mu m$	179.4°	0.280	0.277
	$\tau = 22, r_{\mathrm{eff}} = 10\mu m$	179.4°	0.272	0.259
	$\tau = 14, r_{\mathrm{eff}} = 10\mu m$	179.3°	0.215	0.201
ice cloud	$\tau = 22, r_{\mathrm{eff}} = 40\mu m$	173.8°	0.227	0.229
	$\tau = 22, r_{\mathrm{eff}} = 10\mu m$	173.8°	0.227	0.229
	$\tau = 14, r_{\mathrm{eff}} = 10\mu m$	173.8°	0.227	0.229

The values of the identification parameters as presented in Eq. 2 and Eq. 3 for the radiances shown in Fig. 1 are listed in Tab. 1. With the help of the two identification parameters it is possible to distinguish between ice and liquid water clouds. The glory serves as distinction criterion which could be identified in all cases. The position of the local maximum of the liquid water cloud radiances does not change much even when varying effective radius and cloud optical thickness. The strength of the glory, however, does vary. In case of an effective radius of 4 µm the difference between $I_{\max} - 0.01 \cdot I_{\max}$ and $I_{173°-180°}$ equals 0.003 $\mathrm{W\,m^{-2}\,nm^{-1}\,sr^{-1}}$. An effective radius of 10 µm yields a difference between $I_{\max} - 0.01 I_{\max}$ and $I_{173°-180°}$ of 0.14 $\mathrm{W\,m^{-2}\,nm^{-1}\,sr^{-1}}$ (τ = 14) and 0.13 $\mathrm{W\,m^{-2}\,nm^{-1}sr^{-1}}$ (τ = 22) respectively.

On the basis of the values of $I_{\max} - 0.01 \cdot I_{\max}$ and $I_{173°-180°}$ it is possible to state if the optical thickness of boundary layer clouds determines how large the detected radiances are. The parameters do not show any sensitivity regarding changes of cloud optical thickness and effective radius in case of ice clouds.

With the help of a test dataset consisting of 480 images taken by the camera the algorithm was tested. The dataset consisted of images taken on the 6th of May 2014 out of which 300 images showed a closed cloud cover below the aircraft and 180 images showed partly broken clouds or optical thin clouds. For a closed cloud cover of optical thick clouds the two proposed criteria (Eq. 1 and Eq. 2) are sufficient. To identify broken and optical thin liquid water clouds respectively additional criteria have to be defined: the ratio between local minimum and maximum of the scattering angle dependent radiance between 173° and 180°, the ratio between the local minimum and the mean of the radiance between 172° and 174° and the standard deviation between 170° - 173°. The criteria determined from the analyses of the test dataset are:

$$0.015 < 1 - \frac{I_{\min}}{I_{\max}} < 0.11 \quad (4)$$

$$-3 < \left(1 - \frac{I_{\min}}{\bar{I}_{172°-174°}}\right) \cdot 1000 < 20 \quad (5)$$

$$\sigma_{170°-173°} < 4.0 \text{ mW m}^{-2} \text{ nm}^{-1} \text{sr}^{-1} \quad (6)$$

All five criteria must be fulfilled for a glory to be identified. Analogous to Eq. (3), the ratio between local minimum and local maximum is a measure for the strength of the glory. Despite that, this criterion is not redundant as tests showed. The ratio of $I_{\min}$ to $I_{172°-174°}$ is a measure of the variation of the scattering angle dependent radiance between 172° and 180°. The variation is low, if the value of $\left(1 - \frac{I_{\min}}{\bar{I}_{172°-174°}}\right) \cdot 1000$ is close to 0.0. The standard deviation between 170° and 173° allows drawing conclusions about the clouds homogeneity.

Tab. 1 and Tab. 2 show the values of the identification parameters for the simulations of radiances of pure liquid water and pure ice clouds. Again there are only minor differences between the simulated radiances of ice clouds after varying effective radius and cloud optical thickness. Since the differences were only minor, just one example of scattering angle dependent radiance of ice clouds was plotted in Fig. 1. With varying cloud optical thickness and varying effective radius changes in the parameters for liquid water clouds could be observed. Since simulated radiances were analysed the cloud was homogeneous and, therefore, the standard deviation was low in all cases. Similar to Tab. 1 the values show that the difference between local minimum and maximum of radiance is smaller for an effective radius of 4 µm ($1 - \frac{I_{\min}}{I_{\max}} \approx 0.07$) than for 10 µm. For these clouds $1 - \frac{I_{\min}}{I_{\max}}$ is approximately 0.11 ($\tau = 14$) or 0.10 ($\tau = 22$) respectively.

Tab. 2 Values of identification criteria derived from test dataset for simulations

		$1 - \frac{I_{\min}}{I_{\max}}$	$\left(1 - \frac{I_{\min}}{I_{172°-174°}}\right) \cdot 10^3$	$\sigma_{170°-173°}$ [mWm^{-2} nm^{-1} sr^{-1}]
liquid water cloud	$\tau = 22, r_{eff} = 4\mu m$	0.0714	1.3	1.60
	$\tau = 22, r_{eff} = 10\mu m$	0.0981	0.4	0.56
	$\tau = 14, r_{eff} = 10\mu m$	0.1079	1.0	0.50
ice cloud	$\tau = 22, r_{eff} = 40\mu m$	0.0001	0.1	0.20
	$\tau = 22, r_{eff} = 10\mu m$	0.0001	0.2	0.20
	$\tau = 14, r_{eff} = 10\mu m$	0.0001	0.2	0.20

In case of the simulated radiances of the ice clouds the local maxima of the radiance are relatively weak compared to the maxima in case of liquid water clouds. The difference between local extrema is almost negligible. This can be seen in Tab. 1 and Tab. 2 and in Fig. 1.

5. Application on measurement examples

During the application of the proposed algorithm on measured data, cloud inhomogeneities

may lead to difficulties. To test the algorithm it was applied to several single images taken by the camera.

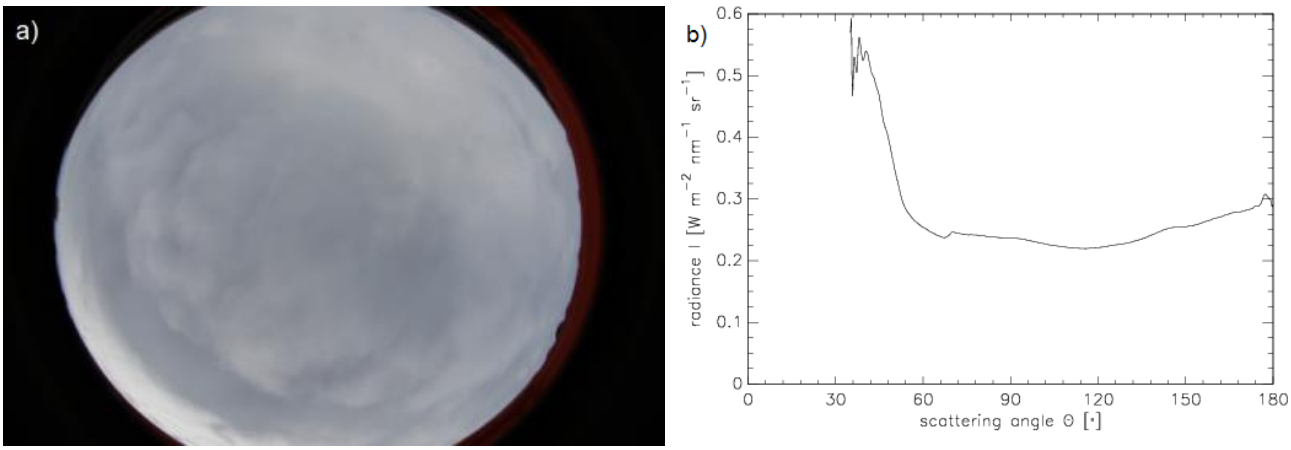

Fig. 2 Image taken by camera (a) and scattering angle dependent radiance (b) at 6 May 2014 at 17:21:16 UTC

An example of a closed boundary cloud layer which appears relatively homogeneously is shown in Fig. 2. This figure shows the image taken by the Canon camera and the corresponding scattering angle dependent radiance of 6 May 2014 at 17:21:16 UTC. The obtained identification parameters are listed in Tab. 3.

The comparison of the parameters with the constraints obtained by analysing simulations and measurements shows that a glory is detected in Fig. 2. In this case the glory could already be identified correctly with the help of the two parameters derived from simulations. Fig. 3 displays both the image and the corresponding scattering angle dependent radiance of 6 May 2014 at 19:49:36 UTC. The image shows clouds with a relatively weak glory but the glory is still detectable in the radiances. The values of the parameters lie within the defined constraints and are shown in Tab. 3.

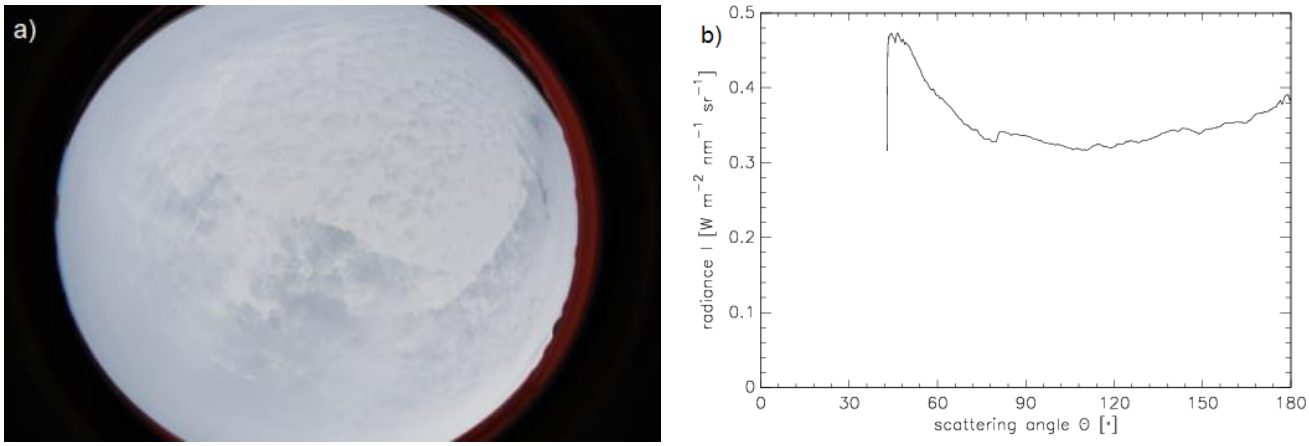

Fig. 3 Image taken by camera (a) and scattering angle dependent radiance (b) at 6 May 2014 at 19:49:36 UTC

An example of a cloud without a glory hence an ice cloud is given in the image of 6 May 2014 at 19:39:52 UTC (Fig. 4). In the image as well as the scattering angle dependent

radiance show no glory whatsoever. Therefore it has to be assumed that at said time the underlying cloud was an ice cloud. The criteria are given in Tab. 3.

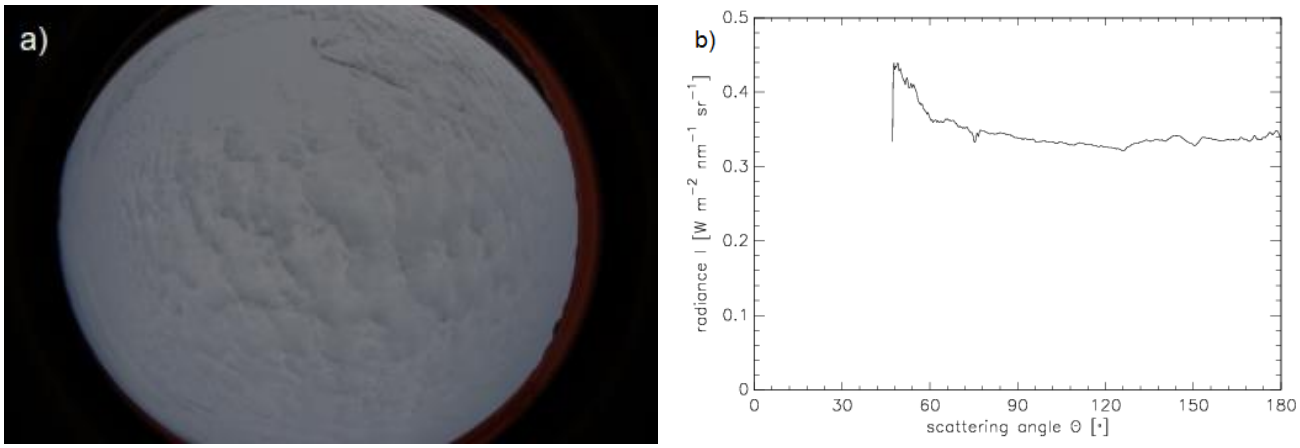

Fig. 4 Image taken by camera (a) and scattering angle dependent radiance (b) at 6 May 2014 at 19:39:52 UTC

This example also gives a handy illustration why the two criteria derived from simulations proved to be insufficient and additional criteria had to be defined. Both the scattering angle of the local maximum and the comparison of the local maximum with the mean of the radiance between 173° and 180° suggest the existence of a glory. Since the ratios of local maximum and minimum and of the local minimum and the mean between 172° and 174° do not correspond to values within the defined constraints, Fig. 4 shows an ice cloud.
On 6 May 2014 at 19:56:16 UTC there was no cloud below the aircraft, as can be seen in Fig. 5. The scattering angle dependent radiance shows a higher variability especially in the section between 170° and 180°. The standard deviation between 170° and 173° of 23.0 mW m^{-2} nm^{-1} sr^{-1} exceeds the threshold of 4.0 mW m^{-2} nm^{-1} sr^{-1}.

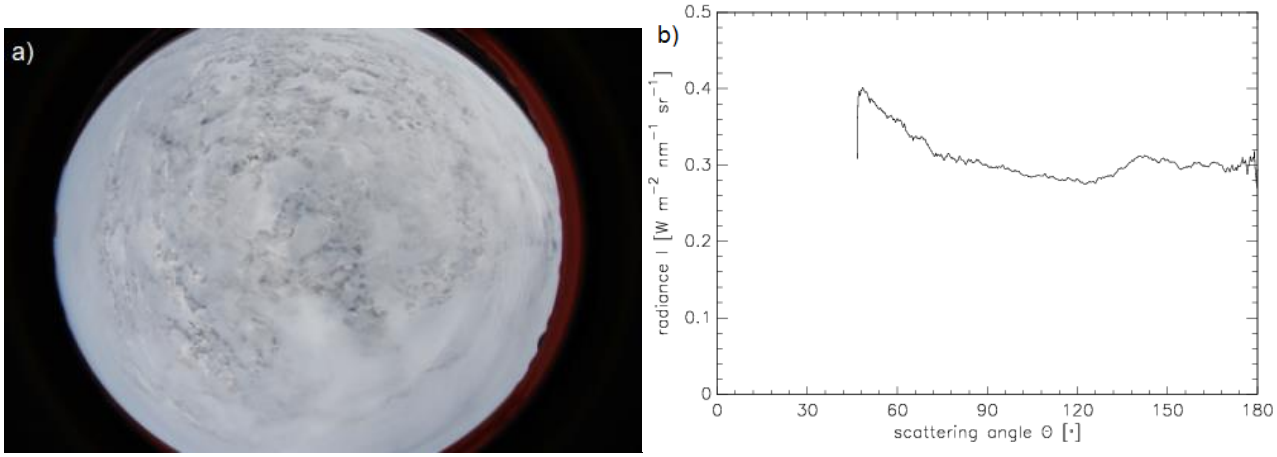

Fig. 5 Image taken by camera (a) and scattering angle dependent radiance (b) at 6 May 2014 at 19:56:16 UTC

Tab. 3 Values of identification criteria for the images shown in Fig. 2-5

Fig.	Time (UTC)	$\theta_{\max}$	$I_{\max} - 0.01 I_{\max}$ [$\mathrm{Wm^{-2}\,nm^{-1}\,sr^{-1}}$]	$\bar{I}_{173°-180°}$ [$\mathrm{Wm^{-2}\,nm^{-1}\,sr^{-1}}$]	$1 - \frac{I_{\min}}{I_{\max}}$	$\left(1 - \frac{I_{\min}}{I_{172°-174°}}\right) 10^3$	$\sigma_{170°-173°}$ [$\mathrm{mWm^{-2}nm^{-1}sr^{-1}}$]
2	17:21:16	177.3°	0.304	0.295	0.0730	2.1	1.24
3	19:49:36	179.1°	0.386	0.381	0.0480	-1.0	1.34
4	19:39:52	178.2°	0.344	0.343	0.0146	-13.8	1.97
5	19:56:16	179.5	0.306	0.300	0.0750	27.1	23.0

6. Conclusion

The glory is an optical phenomenon consisting of concentrical, coloured rings around the anti-solar point caused by scattering on spherical particles with a radius between 4 µm and 25 µm (Laven, 2005). The size of the rings is inverse proportional to the size of the droplets.
Images taken on 6 May 2014 during the campaign RACEPAC with a calibrated Canon digital camera equipped with a 180° fish-eye lens were analysed for the occurrence of glories. To identify glories from measurements of scattering angle dependent radiance the following five criteria within tested boundary values were used:

- Position of local maximum between 173°-180°
- Comparison of local maximum with the mean between 173°-180°
- Ratio of local minimum to local maximum (both between 173°-180°)
- Ratio of local minimum to mean between 172°-174°
- Standard deviation between 170°-173°

With the help of the proposed criteria it is possible to identify glories at the top of arctic boundary layer clouds and therefore to identify the dominating phase at the cloud top. The proposed criteria should be applied to further measurements of scattering angle dependent radiance in order to improve the criteria.
Since both mixed-phase clouds and liquid water clouds feature a glory at the cloud top, a distinction between these two cloud types is not possible. To differentiate between mixed-phase and liquid water clouds the use of methods such as spectral reflectivity measurements, which rely on a weighting function which penetrates deeper into the cloud should be considered.

7. References

Bréon, F.-M. and Goloub, P.: Cloud droplet effective radius from spaceborne polarization measurements,
Geophys. Res. Lett., 25, 1879-1882, doi:10.1029/98GL01221, 1998.

Buras, R., Dowling, T. and Emde, C.: New secondary-scattering correction in DISORT with increased efficiency for forward scattering, J. Quant. Spectrosc. Ra., 112, 2028 - 2034, doi:http://dx.doi.org/10. 1016/j.jqsrt.2011.03.019, 2011.

Ehrlich, A., Wendisch, M., Bierwirth, E., Gayet, J.-F., Mioche, G., Lampert, A. and Mayer, B.: Evidence of ice crystals at cloud top of Arctic boundary-layer mixed-phase clouds derived from airborne remote sensing, Atmos. Chem. Phys., 9, 9401-9416, doi:10.5194/acp-9-9401-2009, 2009.

Ehrlich, A., Bierwirth, E., Wendisch, M., Herber, A. and Gayet, J.-F.: Airborne hyperspectral observations of surface and cloud directional reectivity using a commercial digital camera, Atmos. Chem. Phys., 12, 3493-3510, doi:10.5194/acp-12-3493-2012, 2012.

Emde, C., Buras-Schnell, R., Kylling, A., Mayer, B., Gasteiger, J., Hamann, U., Kylling, J., Richter, B., Pause, C., Dowling, T. and Bugliaro, L.: The libRadtran software package for radiative transfer calculations (version 2.0.1), Geosci. Model Dev., 9, 1647-1672, doi:10.5194/gmd-9-1647-2016, 2016.

Key, J. R., Yang, P., Baum, B. A. and Nasiri, S. L.: Parameterization of shortwave ice cloud optical properties for various particle habits, .J Geophys. Res.-Atmos., 107, AAC 7-1-AAC 7-10, doi:10.1029/2001JD000742, 2002.

Korolev, A. V. and Isaac, G.: The effect of spatial averaging on the relative humidity and phase composition of cloud, in: Proceedings of the 15th International Conference on Clouds and Precipitation, Int. Comm. on Clouds and Precip., Cancun, 2008.

Korolev, A. V., Isaac, G. A., Cober, S. G., Strapp, J. W. and Hallett, J.: Microphysical characterization of mixed-phase clouds, Q. J. Roy. Meteor. Soc., 129, 39-65, doi:10.1256/qj.01.204, 2003.

Laven, P.: Atmospheric glories: simulations and observations, Appl. Opt., 44, 5667-5674, doi:10.1364/AO.44.005667, 2005.

Mioche, G., Jourdan, O., Ceccaldi, M. and Delanoé, J.: Variability of mixed-phase clouds in the Arctic with a focus on the Svalbard region: a study based on spaceborne active remote sensing, Atmos. Chem. Phys., 15, 2445-2461, doi:10.5194/acp-15-2445-2015, 2015.

Wendisch, M., Yang, P. and Ehrlich, A.: Amplified climate changes in the Arctic: Role of clouds and atmospheric radiation., in: Sitzungsberichte der Sächsischen Akademie der Wissenschaften zu Leipzig. Mathematisch Naturwissenschaftliche Klasse, 1-34 Vol. 132, S. Hirzel Verlag, Stuttgart/Leipzig, 2013. 44